

Finite-temperature hydrodynamics for one-dimensional Bose gases: Breathing mode oscillations as a case study

I. Bouchoule,¹ S. S. Szigeti,^{2,3} M. J. Davis,² and K. V. Kheruntsyan²

¹*Laboratoire Charles Fabry, Institut d'Optique, CNRS, Université Paris Sud 11,
2 Avenue Augustin Fresnel, F-91127 Palaiseau Cedex, France*

²*University of Queensland, School of Mathematics and Physics, Brisbane, Queensland 4072, Australia*

³*ARC Centre for Engineered Quantum Systems, University of Queensland, Brisbane, Queensland 4072, Australia*

(Dated: December 3, 2024)

We develop a finite-temperature hydrodynamic approach for a harmonically trapped one-dimensional quasi-condensate and apply it to describe the phenomenon of frequency doubling in the breathing-mode oscillations of its momentum distribution. The doubling here refers to the oscillation frequency relative to the oscillations of the real-space density distribution, invoked by a sudden confinement quench. We find that the frequency doubling is governed by the quench strength and the initial temperature, rather than by the crossover from the ideal Bose gas to the quasicondensate regime. The hydrodynamic predictions are supported by the results of numerical simulations based on a finite-temperature c -field approach, and extend the utility of the hydrodynamic theory for low-dimensional quantum gases to the description of finite-temperature systems and their dynamics in momentum space.

PACS numbers: 03.75.Kk, 67.85.-d, 05.30.Jp

Hydrodynamics is a powerful and broadly applicable approach for characterizing the collective nonequilibrium behavior of a wide range of classical and quantum fluids, including Fermi liquids, liquid helium, and ultra-cold atomic Bose and Fermi gases [1–6]. For ultra-cold gases, the hydrodynamic approach has been particularly successful in describing the breathing (monopole) and higher-order (multipole) collective oscillations of harmonically trapped three-dimensional (3D) Bose-Einstein condensates [2, 6, 7]. For condensates near zero temperature, the applicability of the approach stems from the fact that for long-wavelength (low-energy) excitations the hydrodynamic equations are essentially equivalent to those of superfluid hydrodynamics, which in turn can be derived from the Gross-Pitaevskii equation for the order parameter. For partially condensed samples at finite temperatures, the hydrodynamic equations should be generalized to the equations of two-fluid hydrodynamics, where the applicability of the approach to the normal (thermal) component of the gas is justified by fast thermalization times due to collisional relaxation [3, 8].

In contrast to 3D systems, the applicability of the hydrodynamic approach to 1D Bose gases is not well established. Firstly, in the thermodynamic limit 1D Bose gases lack the long-range order required for superfluid hydrodynamics to be *a priori* applicable. Secondly, the very notion of local thermalisation, required for the validity of collisional hydrodynamics of normal fluids, is questionable due to the underlying integrability of the uniform 1D Bose gas model [9]. Despite these reservations, the hydrodynamic approach has already been applied to zero-temperature ($T = 0$) dynamics of 1D Bose gases in various scenarios [10–14] (for related experiments, see [15–17]). The comparison of hydrodynamic predictions with exact theoretical results is challenging. In Ref. [13], time-dependent density matrix renormalization group simulations of the collision of 1D Bose gases at $T = 0$ found

reasonable agreement with the hydrodynamic approximation, although the latter failed to predict short wavelength dynamics such as shock waves. An alternative approximate approach, based on the conservation of Lieb-Liniger rapidities, has been applied to describe the free expansion dynamics of a $T = 0$ 1D gas [18] and was able to reproduce the hydrodynamic results for very weak and very strong interactions.

At finite temperatures finding exact predictions is extremely difficult, and thus developing a hydrodynamic approach is appealing, despite its lack of justification. Here, we develop a finite- T hydrodynamic approach and show that, for breathing-mode oscillations of a harmonically trapped 1D quasicondensate, the predictions agree both with experimental observations [17] and numerical simulations of a finite-temperature c -field methodology [19, 20]. More remarkably, our hydrodynamic approach not only adequately describes the dynamics of the density distribution of the gas (the standard observable of the hydrodynamic theory), but it can be also used to describe the dynamics of the *momentum distribution*.

Reference [17] experimentally studied confinement quenches of a finite- T 1D Bose gas. The key finding was the phenomenon of frequency doubling in the oscillations of the momentum distribution relative to the breathing-mode oscillations of the real-space density profile. Deep in the quasicondensate regime [21–26] a periodic narrowing of the momentum distribution occurred at twice the frequency of the breathing-mode of the density profile. Although the gas was at finite temperature, the dynamics in momentum space are well-described by a simple zero-temperature classical hydrodynamic approach, wherein the frequency doubling was interpreted as a result of a self-reflection mechanism due to the mean-field interaction energy barrier. In contrast, no frequency doubling was observed in the nearly ideal Bose gas regime. In the absence of an adequate theoretical treatment for $T > 0$, one could naively conclude that the crossover

from frequency doubling to no doubling is governed by the crossover from the quasicondensate regime to the ideal Bose gas regime. However, this picture is incorrect, and as we show here, the frequency doubling crossover can occur even within the quasicondensate regime, and is governed by both the strength of the quench and the temperature.

1. Hydrodynamic equations and evolution of the density distribution.—The hydrodynamic approach relies on the local density approximation (LDA) and assumes that the 1D system can be divided into small locally uniform slices, each of which is in thermal equilibrium in the local moving frame. Moreover, one can assume that heat transfer between the slices is negligible for long-wavelength excitations [27], which implies that each slice undergoes isentropic (de)compression. The hydrodynamic description of this system is [1]

$$\partial_t \rho + \partial_x(\rho v) = 0, \quad (1a)$$

$$\partial_t v + v \partial_x v = -\frac{1}{m} \partial_x V(x, t) - \frac{1}{m \rho} \partial_x P, \quad (1b)$$

$$\partial_t s + v \partial_x s = 0, \quad (1c)$$

where $\rho(x, t)$ is the local 1D density of the slice at position x , $v(x, t)$ is the respective hydrodynamic velocity, $s(x, t)$ is the entropy per particle, $P(x, t)$ is the pressure, m is the mass of the constituent particles, and $V(x, t)$ is the external trapping potential which we assume is harmonic, $V(x, t) = \frac{1}{2}m\omega(t)^2 x^2$, of frequency $\omega(t)$.

We now apply the hydrodynamic approach to describe the post-quench dynamics induced by the following scenario. Initially the atomic cloud with density profile $\rho_0(x)$ is in thermal equilibrium at temperature T_0 in the trap of frequency ω_0 . Subsequently, at time $t = 0$, the trap frequency is suddenly changed to ω_1 . To characterize the ensuing dynamics in different regimes of the 1D Bose gas, we introduce the dimensionless interaction parameter $\gamma_0 = mg/\hbar^2 \rho_0(0)$ and the dimensionless temperature $t_0 = 2\hbar^2 k_B T_0/mg^2$ [28, 29], where g is the coupling strength of the pairwise δ -function interaction potential. The solutions of the HDEs (1a)–(1c) describing this harmonic-confinement quench depend only on the thermodynamic equation of state of the gas. In each of the following three cases, (i) – ideal gas regime ($t_0, \gamma_0^{3/2} t_0 \gg 1$), (ii) – strongly interacting or Tonks-Girardeau regime ($\gamma_0, 1/t_0 \gg 1$), and (iii) – quasicondensate regime ($\gamma_0, \gamma_0^{3/2} t_0 \ll 1$), the solutions reduce to scaling equations of the form

$$\rho(x, t) = \rho_0(x/\lambda(t))/\lambda(t), \quad v(x, t) = x\dot{\lambda}(t)/\lambda(t), \quad (2)$$

$$T(t) = T_0/\lambda(t)^{\nu+1}. \quad (3)$$

The breathing-mode oscillations of the density profile are described by the scaling parameter $\lambda(t)$ [with $\dot{\lambda} \equiv d\lambda(t)/dt$, $\lambda(0) = 1$, and $\dot{\lambda}(0) = 0$], which satisfies

$$\ddot{\lambda} = -\omega_1^2 \lambda + \omega_0^2 / \lambda^{2\nu+1}, \quad (4)$$

where the value of ν in each case is given below.

(i) *Ideal gas regime* ($t_0, \gamma_0^{3/2} t_0 \gg 1$): In this case $\nu = 1$, and the validity of the above scaling solutions can be demonstrated

using a dimensional analysis of the equation of state (see Ref. [30]), which we note is also applicable to an ideal Fermi gas. Equation (4) in this regime has an explicit analytic solution,

$$\lambda(t) = \sqrt{(1 + \epsilon/2) \cos(2\omega_1 t) - \epsilon/2}. \quad (5)$$

This corresponds to harmonic oscillations of the mean squared width of the density profile, occurring at frequency $\omega_B = 2\omega_1$, with $\epsilon \equiv (\omega_0/\omega_1)^2 - 1$ characterizing the quench strength. This result coincides with that for a noninteracting gas obtained from a single-particle picture. The fact that the hydrodynamic approach, which *a priori* assumes sufficient collisions to ensure local thermal equilibrium, agrees with the results for a noninteracting gas is specific to the harmonic-confinement quench scenario considered here and is accidental.

(ii) *Strongly interacting regime* ($\gamma_0, 1/t_0 \gg 1$): Here, the equation of state is that of an ideal Fermi gas so that the previous ideal gas results apply, and Eqs. (2)–(4) are fulfilled with $\nu = 1$. The breathing mode oscillations of the momentum distribution of a finite-temperature Tonks-Girardeau gas will be discussed elsewhere [31].

(iii) *Quasicondensate regime* ($\gamma_0, \gamma_0^{3/2} t_0 \ll 1$): In this case $\nu = 1/2$, and the validity of the scaling solutions (2) can be demonstrated using the equation of state $P = \frac{1}{2}g\rho^2$. The latter can be derived from the quasicondensate chemical potential $\mu = g\rho$ and the Gibbs-Duhem relation $\rho = (\partial P/\partial\mu)_T$. For a weak quench, $\epsilon \ll 1$, the solution to Eq. (4) oscillates at frequency $\omega_B \simeq \sqrt{3}\omega_1$ and is nearly harmonic with an amplitude of $\lambda(t = \pi/\omega_B) - 1 \simeq 2\epsilon/3$ [32]. According to Eq. (2), the density profile breathes self-similarly, maintaining its initial Thomas-Fermi parabolic shape, $\rho_0(x) = \rho_0(0)(1 - x^2/X_0^2)$ for $x \leq X_0$ [and $\rho_0(x) = 0$ otherwise], with $X_0 = \sqrt{2g\rho_0(0)/m\omega_0^2}$. Finite-temperature effects are not seen in the dynamics of the density distribution $\rho(x, t)$ [33] because in this regime the equation of state does not depend on the temperature. However, as we show below, such effects can be revealed in the dynamics of the momentum distribution.

2. Dynamics of the momentum distribution.—Let us consider a slice of the gas in the region $[x, x + dx]$ of density $\rho(x, t)$, velocity $v(x, t)$, and entropy per particle $s(x, t)$. In the laboratory frame its momentum distribution is $\bar{n}(\rho, s, k - mv/\hbar)$, where \bar{n} is the equilibrium momentum distribution of a homogeneous gas, which we normalize to $\int dk \bar{n}(\rho, s; k) = \rho$. The total momentum distribution is then given by

$$n(k, t) = \int dx \bar{n}(\rho, s; k - mv(x, t)/\hbar). \quad (6)$$

There are two contributions to $n(k, t)$: the hydrodynamic velocity field and the contribution of thermal velocities, which have different effects on the breathing mode oscillations. In order to see the sole effect of the hydrodynamic velocity field, let us first disregard the effect of the thermal velocities, taking $\bar{n}(\rho, s; k - mv(x, t)/\hbar) = \rho\delta(k - mv(x, t)/\hbar)$, where $\delta(k)$ is the Dirac delta function. If a scaling solution as in Eq. (2)

exists, the hydrodynamic component of the momentum distribution evolves according to

$$n_h(k, t) = \frac{\hbar}{m|\dot{\lambda}|} \rho_0 \left(\frac{\hbar k}{m\dot{\lambda}} \right). \quad (7)$$

For oscillatory $\lambda(t)$, this implies that $n_h(k, t)$ collapses to a zero-width distribution *twice* per position-space density breathing cycle: when the width of the cloud in real space is both largest and smallest, both corresponding to $\dot{\lambda} = 0$. Therefore, the oscillations of the hydrodynamic contribution to the momentum distribution will always display frequency doubling.

Now consider the additional contribution of thermal velocities to $n(k, t)$, which changes as each slice undergoes isentropic compression and decompression during the breathing cycle. Since one expects the momentum width to be a monotonically increasing function of the compression factor, the thermal momentum width of each slice [and hence of the overall momentum distribution $n(k, t)$] is expected to oscillate out-of-phase relative to the width of the real-space density profile, but at the same breathing frequency ω_B .

The evolution of the overall momentum distribution $n(k, t)$ results from the combined contribution of the hydrodynamic and thermal parts. For a near-ideal gas at $T > 0$ this leads to a somewhat fortuitous cancellation of the hydrodynamic velocity field by the thermal component, and so the total momentum distribution always oscillates at $\omega_B = 2\omega_1$ (see Ref. [30]) and never displays frequency doubling, consistent with the single-particle picture.

The situation is different, however, in the quasicondensate regime. The momentum distribution of a homogeneous quasicondensate of density ρ and temperature T , for wavelengths in the phononic regime (i.e., $k \ll \sqrt{mg\rho/\hbar}$), is given by a Lorentzian $\bar{n}(\rho, s; k) = (2\rho l_\phi/\pi) / [1 + (2l_\phi k)^2]$ [34, 35], where $l_\phi = \hbar^2 \rho / m k_B T$. Substituting this result into Eq. (6), we obtain the full momentum distribution of the trapped gas,

$$n(k, t) = \frac{1}{\pi} \int dx \frac{2l_\phi(x, t)\rho(x, t)}{1 + 4[l_\phi(x, t)]^2[k - mv(x, t)/\hbar]^2}, \quad (8)$$

where $l_\phi(x, t) = \hbar^2 \rho(x, t) / m k_B T(t)$. According to the scaling solutions (2) and (3) with $\nu = 1/2$ (see also [30]), $l_\phi(x, t)$ evolves as

$$l_\phi(x, t) = \sqrt{\lambda} l_\phi^{(0)} \tilde{\rho}_0(x/\lambda), \quad (9)$$

where $\tilde{\rho}_0(x) = 1 - x^2/X_0^2$ is the scaled initial density profile and $l_\phi^{(0)} = \hbar^2 \rho_0(0) / m k_B T_0 = 2[\rho_0(0)\gamma_0^2 t_0]^{-1}$.

Combining the scaling solution for $l_\phi(x, t)$ with that for $\rho(x, t)$, and changing variables to $u = x/\lambda X_0$ in Eq. (8), leads to the following final result

$$n(k, t) = B \sqrt{\tilde{\lambda}} \int_{-1}^1 du \frac{(1 - u^2)^2}{1 + 4\tilde{\lambda}(1 - u^2)^2 \left(\tilde{k} - \frac{\omega_1}{\omega_0} A \dot{\tilde{\lambda}} u \right)^2}. \quad (10)$$

Here, $\tilde{k} = l_\phi^{(0)} k$, $A = m\omega_0 X_0 l_\phi^{(0)} / \hbar = \sqrt{8}/\gamma_0^{3/2} t_0$, and $B = 2\rho_0(0)l_\phi^{(0)} X_0 / \pi$ is a normalization factor. In addition, we have introduced a dimensionless time $\tau \equiv \omega_1 t$, so that the dimensionless functions $\tilde{\lambda}(\tau) \equiv \lambda(\tau/\omega_1)$ and $\dot{\tilde{\lambda}} = d\tilde{\lambda}/d\tau$, obtained from Eq. (4), depend only on the ratio ω_1/ω_0 , or equivalently only on the quench strength $\epsilon = (\omega_0/\omega_1)^2 - 1$. Thus, for a given ϵ , the evolution of $n(k, t)$ is governed solely by the dimensionless parameter A , which itself depends only on the initial intensive parameters γ_0 and t_0 . Note that $A \gg 1$ in the quasicondensate regime where $\gamma_0^{3/2} t_0 \ll 1$ [25, 28].

Using Eq. (10) for a given A and quench strength ϵ , we can now compute the evolution of the full momentum distribution and its half width at half maximum (HWHM); see Figs. 1(a)–(b). The HWHM can then be fitted with a sum of two sinusoidal functions: the fundamental mode oscillating at ω_B ($\simeq \sqrt{3}\omega_1$, for $\epsilon \ll 1$) and the first harmonic oscillating at $2\omega_B$, with amplitudes c_1 and c_2 , respectively. Defining the weight of the fundamental mode as $K = c_1^2/(c_1^2 + c_2^2)$, we identify the frequency doubling phenomenon with $K \ll 1$, whereas $K \simeq 1$ corresponds to the absence of doubling. The doubling crossover can, therefore, be defined as the value of $A = A_{\text{fd}}$ for which $K = 1/2$. As we show in [30], for small quench amplitudes one expects the frequency doubling to occur for $A\sqrt{\epsilon} \gg 1$, while for $A\sqrt{\epsilon} \ll 1$ the thermal effects dominate and the frequency doubling is absent; accordingly, A_{fd} is expected to scale as $A_{\text{fd}} \propto 1/\sqrt{\epsilon}$. Figure 1(c), obtained using Eq. (10) and the fitting procedure described above, confirms this expectation.

In Fig. 1(d) we superimpose the conditions for observing the phenomenon of frequency doubling on the interaction-temperature phase diagram of the 1D Bose gas for two different quenches. As we see, for small enough quench strengths, the crossover from doubling to no doubling lies well within the quasicondensate regime. We therefore conclude that this phenomenon is governed not by the crossover from the ideal Bose gas regime into the quasicondensate regime, but by the competition between the hydrodynamic velocity (which always displays doubling) and the broadening/narrowing of the thermal component of the gas due to adiabatic compression/decompression (which always oscillates at the fundamental frequency ω_B). For very small quenches the initial temperature determines whether doubling occurs, and thus the transition can be observed entirely inside the quasicondensate regime.

Although the applicability of the hydrodynamic theory in this system might be questionable, our analytic results have been benchmarked against finite-temperature c -field simulations whose validity for quasicondensates is well established [19, 20, 37]. Qualitatively, the same behaviour as in Figs. 1(a)–(b) occurs in c -field simulations [36]; quantitatively, the crossover from doubling to no-doubling is in line with the analytic predictions [see Fig. 1(c)]. Moreover, as we argue in Ref. [30], for sufficiently weak confinement (small ω_0), the c -field dynamics are governed by just two dimensionless parameters, A and ϵ , as predicted from the hydrodynamic

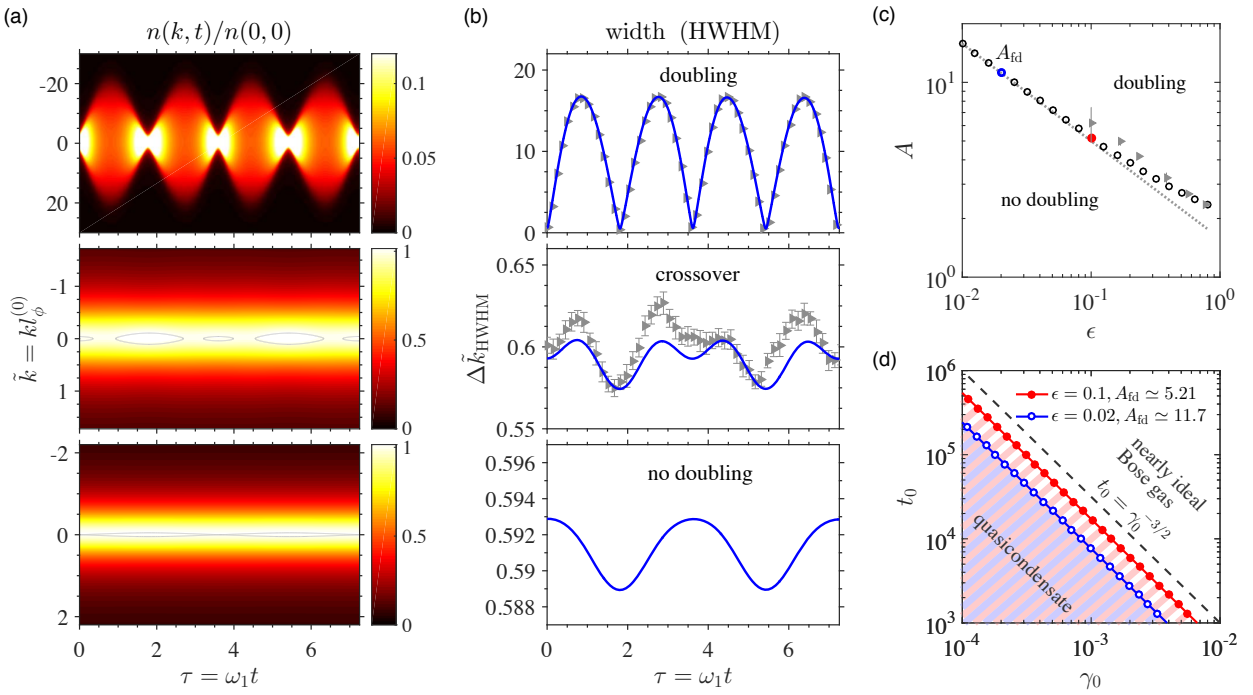


FIG. 1. (Color online). (a) Breathing mode oscillations and (b) the respective widths (HWHM) of the momentum distribution of a harmonically trapped 1D quasicondensate after a confinement quench as a function of the dimensionless time $\tau = \omega_1 t$. The three examples shown in (a) and (b) correspond, respectively, to: $\epsilon = 0.563$, $A = 104$ (with $t_0 = 10^6$ and $\hbar\omega_0/[g\rho_0(0)] = 3.0 \times 10^{-3}$ is c -field simulations) – top row; $\epsilon = 0.101$, $A = A_{\text{fd}} = 5.21$ ($t_0 = 10^3$, $\hbar\omega_0/[g\rho_0(0)] = 1.1 \times 10^{-2}$) – middle row; and $\epsilon = 0.0203$, $A = 3.95$ – bottom row [36]. The grey triangles are the c -field data [30], with the error bars indicating 95% confidence interval. (c) Phase diagram of the frequency doubling phenomenon in the A - ϵ plane; data points (circles) show the doubling crossover values A_{fd} for which the weights of the fundamental and the first harmonics are equal ($K = 1/2$); grey triangles are from c -field simulations. The dotted line is a fit in the region $A > 5$ with a power law $A_{\text{fd}} \simeq 1.58/\sqrt{\epsilon}$ (see text). (d) Frequency doubling conditions superimposed on the equilibrium phase diagram of the 1D Bose gas drawn in terms of the dimensionless temperature (t_0) and interaction strength (γ_0) and covering the quasicondensate and the neighbouring nearly ideal Bose gas regimes. The grey dashed line ($t_0 = \gamma_0^{-3/2}$) corresponds to the crossover between the two regimes. The two lines with filled (red) and open (blue) circles, on the other hand, correspond to the frequency doubling crossover conditions for two different quenches, $\epsilon = 0.1$ and $\epsilon = 0.02$ (the respective data points in (c) are labelled in the same way). The (light red and light blue) shaded areas underneath these lines correspond to the conditions where the frequency doubling occurs.

approach. Overall, the performance of the hydrodynamic theory in modelling the harmonic confinement quench of a finite-temperature quasicondensate is remarkable, given the extent of approximations and assumptions that go into its formulation in the first place.

In summary, we have developed a finite-temperature hydrodynamic approach for a harmonically trapped 1D Bose gas and applied it to the study of breathing mode oscillations in the quasicondensate regime. For problems with a known initial equilibrium momentum distribution, our approach extends the utility of the hydrodynamic theory to describing its subsequent dynamics. The approach allowed us to discern the contribution of the hydrodynamic velocity field and that of thermal excitations, hence explaining the full mechanism behind the phenomenon of frequency doubling in the oscillatory dynamics of the momentum distribution of the gas. Our hydrodynamic predictions are in broad agreement with numerical simulations based on finite-temperature c -field simulations. Future extensions of this work will concern the treatment of breathing mode oscillations in the strongly interacting regime

[31], and could address collective oscillations of 2D and 3D quasicondensates in highly elongated geometries.

K. V. K. acknowledges stimulating discussions with D. M. Gangardt. I. B. acknowledges support by the Centre de Compétences Nanosciences Île-de-France; S. S. S. – by the Australian Research Council Centre of Excellence for Engineered Quantum Systems (grant No. CE110001013); M. J. D. and K. V. K. – by the ARC Discovery Project grants DP160103311 and DP140101763. Numerical simulations were performed using XMDS2 [38] on the University of Queensland School of Mathematics and Physics computer “Obelix”, with thanks to I. Mortimer for computing support.

- [1] L. D. Landau and E. M. Lifshitz, *Fluid Mechanics* (2nd edition, Vol. 6 of A Course of Theoretical Physics, Pergamon Press, Oxford, 1987).
- [2] L. P. Pitaevskii and S. Stringari, *Bose-Einstein Condensation*

(Clarendon Press, Oxford, 2003).

[3] A. Griffin, T. Nikuni, and E. Zaremba, *Bose-Condensed Gases at Finite Temperatures* (Cambridge University Press, Cambridge, 2009).

[4] A. Griffin, W.-C. Wu, and S. Stringari, Phys. Rev. Lett. **78**, 1838 (1997).

[5] Y. Kagan, E. L. Surkov, and G. V. Shlyapnikov, Phys. Rev. A **55**, R18 (1997).

[6] L. Pitaevskii and S. Stringari, Phys. Rev. Lett. **81**, 4541 (1998).

[7] S. Stringari, Phys. Rev. Lett. **77**, 2360 (1996).

[8] L. A. Sidorenkov, M. K. Tey, R. Grimm, Y.-H. Hou, L. Pitaevskii, and S. Stringari, Nature **498**, 78 (2013).

[9] E. H. Lieb and W. Liniger, Phys. Rev. **130**, 1605 (1963).

[10] A. Minguzzi, P. Vignolo, M. L. Chiofalo, and M. P. Tosi, Phys. Rev. A **64**, 033605 (2001).

[11] C. Menotti and S. Stringari, Phys. Rev. A **66**, 043610 (2002).

[12] P. Öhberg and L. Santos, Phys. Rev. Lett. **89**, 240402 (2002); P. Pedri, L. Santos, P. Öhberg, and S. Stringari, Phys. Rev. A **68**, 043601 (2003).

[13] S. Peotta and M. D. Ventra, Phys. Rev. A **89**, 013621 (2014).

[14] S. Choi, V. Dunjko, Z. D. Zhang, and M. Olshanii, Phys. Rev. Lett. **115**, 115302 (2015).

[15] H. Moritz, T. Stöferle, M. Köhl, and T. Esslinger, Phys. Rev. Lett. **91**, 250402 (2003).

[16] E. Haller, M. Gustavsson, M. J. Mark, J. G. Danzl, G. P. R. Hart, and H.-C. Nägerl, Science **325**, 1224 (2009).

[17] B. Fang, G. Carleo, A. Johnson, and I. Bouchoule, Phys. Rev. Lett. **113**, 035301 (2014).

[18] A. S. Campbell, D. M. Gangardt, and K. V. Kheruntsyan, Phys. Rev. Lett. **114**, 125302 (2015).

[19] M. J. Davis, S. A. Morgan, and K. Burnett, Phys. Rev. Lett. **87**, 160402 (2001).

[20] P. B. Blakie, A. S. Bradley, M. J. Davis, R. J. Ballagh, and C. W. Gardiner, Advances in Physics **57**, 363 (2008).

[21] D. S. Petrov, G. V. Shlyapnikov, and J. T. M. Walraven, Phys. Rev. Lett. **85**, 3745 (2000).

[22] S. Richard, F. Gerbier, J. H. Thywissen, M. Hugbart, P. Bouyer, and A. Aspect, Phys. Rev. Lett. **91**, 010405 (2003).

[23] A. H. van Amerongen, J. J. P. van Es, P. Wicke, K. V. Kheruntsyan, and N. J. van Druten, Phys. Rev. Lett. **100**, 090402 (2008).

[24] S. Hofferberth, I. Lesanovsky, B. Fischer, T. Schumm, and J. Schmiedmayer, Nature **449**, 324 (2007).

[25] T. Jacqmin, J. Armijo, T. Berrada, K. V. Kheruntsyan, and I. Bouchoule, Phys. Rev. Lett. **106**, 230405 (2011).

[26] J. Armijo, T. Jacqmin, K. Kheruntsyan, and I. Bouchoule, Phys. Rev. A **83**, 021605 (2011).

[27] As is well known in acoustic physics, the contribution of heat transfer, estimated using a diffusion equation, to local changes of the energy per particle is negligible for long-wavelength deformations.

[28] K. V. Kheruntsyan, D. M. Gangardt, P. D. Drummond, and G. V. Shlyapnikov, Phys. Rev. A **71**, 053615 (2005).

[29] I. Bouchoule, K. V. Kheruntsyan, and G. V. Shlyapnikov, Phys. Rev. A **75**, 031606 (2007).

[30] See the Supplemental Material at <http://link.aps.org/> supplemental/XXX, which contains additional proofs and clarifications of various aspects of the hydrodynamic solutions, as well as the details of *c*-field simulations.

[31] Y. Atas, I. Bouchoule, D. M. Gangardt, and K. V. Kheruntsyan, in preparation.

[32] For a small amplitude quench ($\epsilon \ll 1$), Eq. (4) with $\nu = 1/2$ can be solved using the method of linearization [i.e., expanding $\lambda(t)$ as $\lambda(t) = 1 + \delta\lambda(t)$, with $\delta\lambda(t) \ll \lambda(t)$], yielding $\lambda(t) \simeq 1 + \frac{\epsilon}{3} - \frac{\epsilon}{3} \cos(\sqrt{3}\omega_1 t)$.

[33] According to the quasicondensate equation of state, the last term in the HDE (1b), $\frac{1}{\rho} \partial_x P = g \partial_x \rho$, does not depend on temperature T and is, in fact, the same as for a $T=0$ gas. Therefore, the HDEs for the density and velocity fields decouple from the equation for s and consequently no finite-temperature effects are seen in the dynamics of the real-space density $\rho(x, t)$ and velocity field $v(x, t)$.

[34] M. A. Cazalilla, Journal of Physics B: Atomic, Molecular and Optical Physics **37**, S1 (2004).

[35] I. Bouchoule, M. Arzamasovs, K. V. Kheruntsyan, and D. M. Gangardt, Phys. Rev. A **86**, 033626 (2012).

[36] The regime of Fig. 1(c) is inaccessible in the *c*-field method due to large sampling errors.

[37] M. J. Davis, P. B. Blakie, A. H. van Amerongen, N. J. van Druten, and K. V. Kheruntsyan, Phys. Rev. A **85**, 031604 (2012).

[38] G. R. Dennis, J. J. Hope, and M. T. Johnsson, Computer Physics Communications **184**, 201 (2013).

Supplemental Material

Finite-temperature hydrodynamics for one-dimensional Bose gases: Breathing mode oscillations as a case study

I. Bouchoule,¹ S. S. Szigeti,^{2,3} M. J. Davis,² and K. V. Kheruntsyan²

¹*Laboratoire Charles Fabry, Institut d'Optique, CNRS, Université Paris Sud 11,
2 Avenue Augustin Fresnel, F-91127 Palaiseau Cedex, France*

²*University of Queensland, School of Mathematics and Physics, Brisbane, Queensland 4072, Australia*

³*ARC Centre for Engineered Quantum Systems, University of Queensland, Brisbane, Queensland 4072, Australia*

In this supplemental material we provide further details on the hydrodynamic scaling solutions, as well as a brief description and further results of our c -field simulations.

I. SCALING SOLUTIONS IN THE HYDRODYNAMIC APPROACH

A. Ideal gas regime.

For a uniform ideal gas (either bosonic or fermionic) at temperature T and 1D density $\rho = N/L$, where N is the number of particles and L is length of the confinement box, the only two length scales are the mean interparticle separation ρ^{-1} and the thermal de Broglie wavelength $\Lambda_T = \sqrt{2\pi\hbar^2/(mk_B T)}$; the corresponding energy scales are $\hbar^2\rho^2/m$ and $k_B T$. Using the thermodynamic definition of the 1D pressure, $P = (\partial U / \partial L)_s$, where U is the internal energy, one can apply simple dimensional analysis to write down the equations of state for P and s :

$$P = k_B T \rho F(\hbar^2 \rho^2 / m k_B T), \quad (\text{S1})$$

$$s/k_B = G(m k_B T / \hbar^2 \rho^2). \quad (\text{S2})$$

Here F and G are dimensionless functions of the only dimensionless parameter—the ratio of the two energy scales. With this choice of expression for P , the classical ideal gas law in the high temperature limit is recovered with $F \simeq 1$. For a highly degenerate ideal Fermi gas, on the other hand, the equation of state $P = \hbar^2 \pi^2 \rho^3 / (3m)$ is recovered with $F \simeq (\pi^2/3)(\hbar^2 \rho^2 / m k_B T)$.

Now consider a confinement quench of the gas. Applying the general functional forms of P and s to small (locally uniform) slices of the gas, it can be shown by direct substitution that the scaling solutions, Eqs. (2) and (3) of the main text, satisfy Eqs. (1a) and (1c). For Eq. (1b) first note that Eq. (S1) together with the scaling solutions imply that $P(x, t) = P_0(x/\lambda)/\lambda^3$, where $P_0(x) \equiv P(x, 0)$. Since Eq. (1b) is assumed true at this initial time, then $\partial_x P_0 = -\rho_0(x) \partial_x V(x, 0) = -m\omega_0^2 x \rho_0(x)$. Together with the scaling solutions and Eq. (4), this relation is sufficient to show that Eq. (1b) is true for all times.

B. Scaling solution for the temperature in the quasicondensate regime.

In order to calculate $n(k, t)$ using the hydrodynamic scaling solutions, Eqs. (2) and (4) of the main text, we first need

to determine how the temperature of the gas and hence the phase correlation length $l_\phi = \hbar^2 \rho / (m k_B T)$ evolves during the breathing oscillations. To do this, we first note that the energy of the j th phonon mode in a quantization box of length L is given by $E_j = \hbar k_j c$, where $k_j = \frac{2\pi}{L} j$ is the phonon wave vector and $c = \sqrt{(\partial P / \partial \rho) / m}$ is the speed of sound. Using $P \propto \rho^2$, we find that c scales as $c \propto \rho^{1/2}$ and therefore $E_j \propto L^{-1} \rho^{1/2} \propto \rho^{3/2}$. Consider now an adiabatic compression/decompression cycle for a uniform slice of the gas confined to a box of length L . Such a compression does not change the mean occupation number of the mode j . The mode occupation is given by $n_j \simeq k_B T / E_j$ in the long-wavelength limit and scales as $n_j \propto T / \rho^{3/2}$, whereas $\rho \propto \lambda^{-1}$ according to the scaling solution, Eq. (2). Therefore, during the adiabatic breathing oscillations, the temperature $T(t)$ evolves from the initial value $T(0) \equiv T_0$ to $T(t) = T_0 / \lambda^{3/2}$, i.e., Eq. (3) of the main text with $\nu = 1/2$.

C. Evolution of the momentum distribution for an ideal gas.

Applying the hydrodynamic approach and Eq. (7) of the main text to the ideal gas regime, we first note that the momentum distribution of a uniform ideal gas (normalized to $\int dk \bar{n}(k) = \rho$) is given by $\bar{n}(\rho, s; k) = \mathcal{N}((\hbar^2 k^2 / 2m - \mu) / k_B T)$, where \mathcal{N} is a dimensionless function whose expression depends on the quantum statistics [1]. Since $\mu / k_B T$ is a function of s (in the sense of a thermodynamic equation of state), which itself is a function of $m k_B T / \hbar^2 \rho^2$ [see Eq. (S2)], one can assert that $\mu / (k_B T) = \mathcal{G}(m k_B T / \hbar^2 \rho^2)$, where \mathcal{G} is a dimensionless function. Then, the scaling solutions (2) and (3) of the main text imply that $\mu(x, t) / k_B T(t) = \mathcal{G}[m k_B T(t) / \hbar^2 \rho^2(x, t)] = \mathcal{G}[m k_B T_0 / \hbar \rho_0^2(x/\lambda)] \equiv \mathcal{G}_0(x/\lambda)$, or

$$\mu(x, t) = \mu(x/\lambda, 0) / \lambda^2 = [\mu_0 - \frac{1}{2} m \omega_0^2 (x/\lambda)^2] / \lambda^2, \quad (\text{S3})$$

where μ_0 is the initial chemical potential in the trap center. Substituting $\bar{n}(\rho, s; k)$ along with this expression for $\mu(x, t)$ into Eq. (6) of the main text, and changing variables to $\tilde{x} = \alpha x - \hbar k \lambda \lambda / (m \omega_0^2 \alpha)$, gives

$$n(k, t) = n_0(k/\alpha) / \alpha, \quad (\text{S4})$$

where $n_0(k)$ is the initial momentum distribution of the trapped gas and $\alpha^2 = (\omega_0^2 + \lambda^2 \dot{\lambda}^2) / (\lambda \omega_0)^2$. Using Eq. (5) of the main text, we can explicitly write α as

$$\alpha = \sqrt{[(1 + \epsilon/2) \cos(2\omega_1 t) + \epsilon/2] / (1 + \epsilon)}, \quad (\text{S5})$$

which implies that the momentum distribution of a finite-temperature ideal gas in the hydrodynamic limit oscillates at $\omega_B = 2\omega_1$ and *never* displays frequency doubling. One thus recovers the expected behaviour for an ideal gas, due to the position-momentum symmetry of the underlying harmonic oscillator Hamiltonian. The fact that this result is reproduced within the hydrodynamic approach is a result of a “fortuitous” exact cancelation of the effect of the hydrodynamic velocity field by the thermal component.

D. Scaling of the frequency doubling crossover A_{fd} with the quench strength ϵ .

In this section we make qualitative arguments that provide an understanding of the dominant oscillation regimes in the dynamics of the momentum distribution of a quasi-condensate, and derive an approximate scaling of A_{fd} with ϵ . Let us first introduce typical momentum scales involved in the dynamics. For small-amplitude oscillations, corresponding to $\epsilon \ll 1$, the scaling parameter λ oscillates as $\lambda(t) \simeq 1 + \frac{\epsilon}{3} - \frac{\epsilon}{3} \cos(\sqrt{3}\omega_1 t)$ and therefore the magnitude of $\dot{\lambda}$ is of the order of $\sim \epsilon/\sqrt{3}$. This means that the characteristic hydrodynamic momentum, which can be estimated as $\bar{k}_h \sim mX_0\lambda/\hbar$ from Eq. (7) of the main text, and which can be rewritten as $\bar{k}_h \sim mX_0\epsilon\omega_1/\hbar \sim (\omega_1/\omega_0)A\epsilon/l_\phi^{(0)}$, is of the order of $\bar{k}_h \sim A\epsilon/l_\phi^{(0)}$ for $\epsilon \ll 1$. Compared to this, the characteristic thermal momentum during the compression/decompression cycle oscillates above $\bar{k}_{\text{th}} \sim 1/l_\phi^{(0)}$ with an amplitude variation of $\delta\bar{k}_{\text{th}} \sim \epsilon/l_\phi^{(0)} \ll \bar{k}_{\text{th}}$.

For $A\epsilon \gg 1$, the characteristic hydrodynamic momentum is much larger than both the characteristic thermal momentum and its variation, $\bar{k}_h \gg \bar{k}_{\text{th}}, \delta\bar{k}_{\text{th}}$. Then, as long as one is interested in momenta of the order of \bar{k}_h , the function \bar{n} in Eq. (6) of the main text can be approximated by a δ -function, and therefore the breathing oscillations of the momentum distribution will be dominated by the hydrodynamic phenomenon of frequency doubling.

In the opposite regime of $A\epsilon \ll 1$, the characteristic hydrodynamic momentum is much smaller than the characteristic thermal momentum, $\bar{k}_h \ll \bar{k}_{\text{th}}$, and therefore the above approximation, which neglects the effect of the width of \bar{n} in Eq. (6), breaks down. In this case, the contribution of the hydrodynamic momenta to $n(k, t)$ can instead be estimated via a Taylor series of \bar{n} as powers of $k_h(x, t) = mv(x, t)/\hbar$. In this series, the contribution of the first-order term to the integral vanishes because $\partial\bar{n}/\partial k$ is an even function of x , whereas $k_h(x, t)$ is odd; therefore, the hydrodynamic velocity field has no effect on $n(k, t)$ in this order. The leading-order correction in $n(k, t)$ thus comes from the second-order derivative term, proportional to k_h^2 . To estimate this correction, let us consider the typical variations of the peak value of the momentum distribution $n(0, t)$, which we denote via δn , induced solely by the hydrodynamic momenta. Using $\partial^2\bar{n}/\partial k^2|_{k=0} \sim \rho_0(0)(l_\phi^{(0)})^3$ in Eq. (6), one can find that $\delta n \sim -X_0\rho_0(0)l_\phi^{(0)3}\bar{k}_h^2$, or $\delta n \sim -X_0\rho_0(0)l_\phi^{(0)}(A\epsilon)^2$, where

we have used $\bar{k}_h \sim A\epsilon/l_\phi^{(0)}$. Since the peak value $n(0, t)$ is inversely proportional to the characteristic momentum width W , the hydrodynamic contribution to the typical change (δW) of the momentum width fulfills $\delta W/W \simeq -\delta n/n(0, 0)$. Using $W \sim \bar{k}_{\text{th}} \sim 1/l_\phi^{(0)}$ and $n(0, 0) \sim \rho_0(0)l_\phi^{(0)}X_0$, we then find $\delta W \sim (A\epsilon)^2/l_\phi^{(0)}$. Comparing now this result with the typical variation of the thermal momentum width $\delta\bar{k}_{\text{th}} \sim \epsilon/l_\phi^{(0)}$, we can conclude that the hydrodynamic contribution $\delta W \sim (A\epsilon)^2/l_\phi^{(0)}$ will dominate the thermal contribution if $A \gg 1/\sqrt{\epsilon}$; in this case, one would still observe the phenomenon of frequency doubling. If, on the other hand, $A \ll 1/\sqrt{\epsilon}$, the breathing oscillations will be dominated by the variations of thermal momenta and no frequency doubling will be observed. Accordingly, one can expect the crossover from doubling to no doubling to occur at $A_{\text{fd}} \propto 1/\sqrt{\epsilon}$, with the proportionality factor to be found from the numerical results. From Fig. 1(c) we see that, in the relevant region of $A \gtrsim 5$, A_{fd} scales as $1/\sqrt{\epsilon}$ as expected. Since $A \gg 1$ in the quasi-condensate regime, the frequency doubling crossover requires very small quench strengths ϵ .

II. NUMERICAL SIMULATIONS USING THE *C*-FIELD METHODOLOGY

A. The *c*-field method

The *c*-field, or classical field, method is a proven approach to studying the equilibrium properties and dynamics of Bose gases at finite temperature [2]. The crux of this approach is that modes with large occupation numbers $n_i = k_B T/\varepsilon_i \gg 1$ can be treated as a classical field $\psi_C(x, t)$, where ε_i is the energy of the mode, whose dynamical evolution is well-described by the Gross-Pitaevskii equation (GPE). In contrast, the higher-energy modes are non-classical and sparsely populated, and are treated as an incoherent (thermal) gas. The stochastic projected GPE (SPGPE) methodology approximates this incoherent region as a static finite temperature reservoir [3, 4], whereas the projected GPE (PGPE) methodology entirely neglects the coupling to the higher-energy modes [5, 6].

In order to generate our initial equilibrium state at finite temperature, we used the simple-growth SPGPE:

$$d\psi_C(x, t) = \mathcal{P}_C \left\{ \left[-\frac{i}{\hbar} \mathcal{L}_C + \kappa_{\text{th}}(\mu - \mathcal{L}_C) \right] \psi_C(x, t) dt + \sqrt{2\kappa_{\text{th}}T} dW(x, t) \right\}. \quad (\text{S6})$$

Here \mathcal{P}_C is the projector onto the subspace of classical, highly-occupied modes, the operator \mathcal{L}_C describes the usual GPE dynamics:

$$\mathcal{L}_C \psi_C = \left[-\frac{\hbar}{2m} \frac{\partial^2}{\partial x^2} + \frac{1}{2} m\omega_0^2 x^2 + g|\psi_C|^2 \right] \psi_C, \quad (\text{S7})$$

and $\langle dW^*(x, t) dW(x', t) \rangle = \delta_C(x - x') dt$, where $\delta_C(x)$ is the kernel of the projection operator \mathcal{P}_C , which acts as a Dirac

delta function within the classical region. The growth rate κ_{th} determines the strength of thermal and diffusive damping experienced by particles in the classical region due to the thermal reservoir (held at temperature T and chemical potential μ). Since we are only interested in the equilibrium states generated by Eq. (S6), the value for the damping rate κ_{th} was chosen for computational convenience, rather than on the basis of a physical theory.

After quenching the trapping frequency $\omega_0 \rightarrow \omega_1$, this initial state was evolved using the simpler PGPE [which can be obtained by setting $\kappa_{\text{th}} = 0$ in Eq. (S6)]. Since the details of the interaction with the thermal reservoir have been neglected, the PGPE tends to incorrectly estimate nonequilibrium damping rates [7]. Nevertheless, nonequilibrium properties have been studied with some success, including the collective oscillations of Bose gases [8, 9]; in our case, the precise rate of damping of the breathing mode oscillation is unimportant.

Our numerical simulations were performed within the Hermite-Gauss basis, which is the single-particle eigenbasis of an harmonically-confined Bose gas. This is the natural, most computationally efficient basis, as it well-approximates the higher-energy, sparsely populated modes, thereby allowing a smooth transition between the classical and incoherent regions [10, 11] (see Eq. (39) of [12] for an explicit expression of the SPGPE in the Hermite-Gauss basis). The basis size is in direct proportion to the energy cutoff ε_{cut} that defines the classical region, and it needs to be chosen such that the average occupation of the modes in the classical region is $\gtrsim 1$; in practice our results are insensitive to the precise choice of ε_{cut} . For consistency, we chose the same energy cutoff for both the PGPE evolution after the confinement quench and the SPGPE that generates the initial condition. However, the Hermite-Gauss modes that represent the single-particle eigenbasis depend upon the trapping frequency. This implies that the number of Hermite-Gauss modes used for the PGPE evolution, \tilde{M}_{cut} , is related to the number of modes in the SPGPE evolution M_{cut} via

$$\tilde{M}_{\text{cut}} = \left\lfloor \frac{\omega_1}{\omega_0} (M_{\text{cut}} + \frac{1}{2}) - \frac{1}{2} \right\rfloor, \quad (\text{S8})$$

where $\lfloor x \rfloor$ denotes the integer component of x .

Figure 1 illustrates PGPE evolution of the position density and momentum distributions after a confinement quench in three different parameter regimes. Although the density undergoes breathing oscillations at frequency $\omega_B \simeq \sqrt{3}\omega_1$ in all three cases, the momentum distribution exhibits frequency doubling (top row), a crossover between quasi-doubling and no doubling (middle row), and no frequency doubling (bottom row). This is consistent with the breathing oscillations predicted by our finite-temperature hydrodynamic theory within the quasicondensate regime (see main text).

B. Details for comparison with finite-temperature hydrodynamic theory in the quasicondensate regime

The thermal equilibrium properties of a harmonically trapped Bose gas at temperature T_0 and peak density $\rho_0(0)$

can be parametrized by the three dimensionless quantities $\gamma_0 = mg/[\hbar^2 \rho_0(0)]$, $t_0 = 2\hbar^2 k_B T_0/(mg^2)$, and $\tilde{\omega} \equiv (l_{\text{HO}}/\xi_0) = \hbar\omega_0/[\rho_0(0)]^2$, where $l_{\text{HO}} = \sqrt{\hbar/(m\omega_0)}$ and $\xi_0 = \hbar/\sqrt{mg\rho_0(0)}$ are the harmonic oscillator length scale and healing length, respectively. However, within the classical field approximation only two parameters are required since features on the order of mean interparticle separation $1/\rho_0(0)$ are neglected. Specifically, if the classical field is scaled by $\psi_0 = [mk_B^2 T_0^2/(\hbar^2 g)]^{1/6}$, the length scale by $x_0 = (\hbar^4/(m^2 g k_B T_0))^{1/3}$, and the trapping frequency by $\bar{\omega} = (k_B T_0 \sqrt{mg}/\hbar)^{2/3}/\hbar$, then the thermal action $\int dx (\frac{\hbar^2}{2m} |\partial\psi_C/\partial x|^2 + \frac{1}{2} m\omega_0^2 x^2 |\psi_C|^2 + \frac{g}{2} |\psi_C|^4 - \mu |\psi_C|^2)/(k_B T)$, which determines the grand canonical partition function, depends only on the dimensionless parameters $\eta_0 = [\hbar^2/(mg^2 k_B^2 T_0^2)]^{1/3} \mu$ and $\omega_0/\bar{\omega}$. Equivalently, the gas can be described by the dimensionless parameters $\chi_0 = k_B T/[\hbar \rho_0(0) \sqrt{g \rho_0(0)/m}]$ and $\tilde{\omega} = \hbar \omega/[\rho_0(0)]$; field correlation functions of order m have previously been shown to depend only on χ_0 and $\tilde{\omega}$, provided they are scaled to $\rho_0(0)^m$ and the lengths are scaled to $\hbar^2 \rho_0/(mk_B T)$ (cf. [13, 14] which investigated the parameter dependence within the classical field approximation for a *uniform* Bose gas). For sufficiently weak trapping frequencies $\tilde{\omega} \rightarrow 0$ and drops out of the problem. This occurs if the size of the atomic cloud is much larger than other microscopic correlation lengths of the gas, therefore implying that the local density approximation (LDA) is valid.

Consider now the post-quench dynamics investigated in this paper. They are *a priori* parametrized by the dimensionless parameters γ_0 , $A = \sqrt{8}/\chi_0 = \sqrt{8}/(\gamma_0^{3/2} t_0)$, ϵ , and $\tilde{\omega}$. Within the classical field approximation, if we rescale the PGPE [cf. Eqs. (S6) and (S7)] as done for the equilibrium case, we find that γ_0 drops out. Additionally, we chose parameters for our c -field simulations such that the dynamics only depend upon A and ϵ . That is, we required a sufficiently weak $\tilde{\omega}$ such that the size of the cloud was always much larger than the typical correlation length $l_\phi^{(0)} = \hbar^2 \rho_0(0)/(mk_B T_0)$ (recall that $l_\phi^{(0)}$ is the typical phase correlation length of the gas, itself larger or on the order of the density-density correlation length). Similarly to the equilibrium case, one then expects a dynamical LDA to be valid, ensuring that the parameter $\tilde{\omega}$ is irrelevant. This further fulfilled the high temperature condition required for (S)PGPE, whilst still ensuring that the number of modes was numerically tractable (recall that we also require $\epsilon_{\text{cut}} \sim k_B T_0$).

In order to compute A_{fd} for a given quench strength ϵ , we fixed t_0 and varied A . For each A , K was extracted by fitting $B_1 \exp(-b_1 t) [\sqrt{K} \cos(\nu t) - \sqrt{1-K} \cos(2\nu t)] + B_2 \exp(-b_2 t)$ to the HWHM of the momentum distribution at each time point t (here B_1, B_2, b_1, b_2, ν , and K are free fitting parameters); see the red curves of Fig. 1 for example fits. The rates b_1 and b_2 account for the damping present in the PGPE evolution, which is absent from our hydrodynamic theory. This gave a dataset (A, K) ; the point A_{fd} where $K = 1/2$ was determined by fitting $\frac{1}{2} [\tanh[a(A^{-2/3} - A_{\text{fd}}^{-2/3})] + 1]$ to this dataset, with free fitting parameters a and A_{fd} .

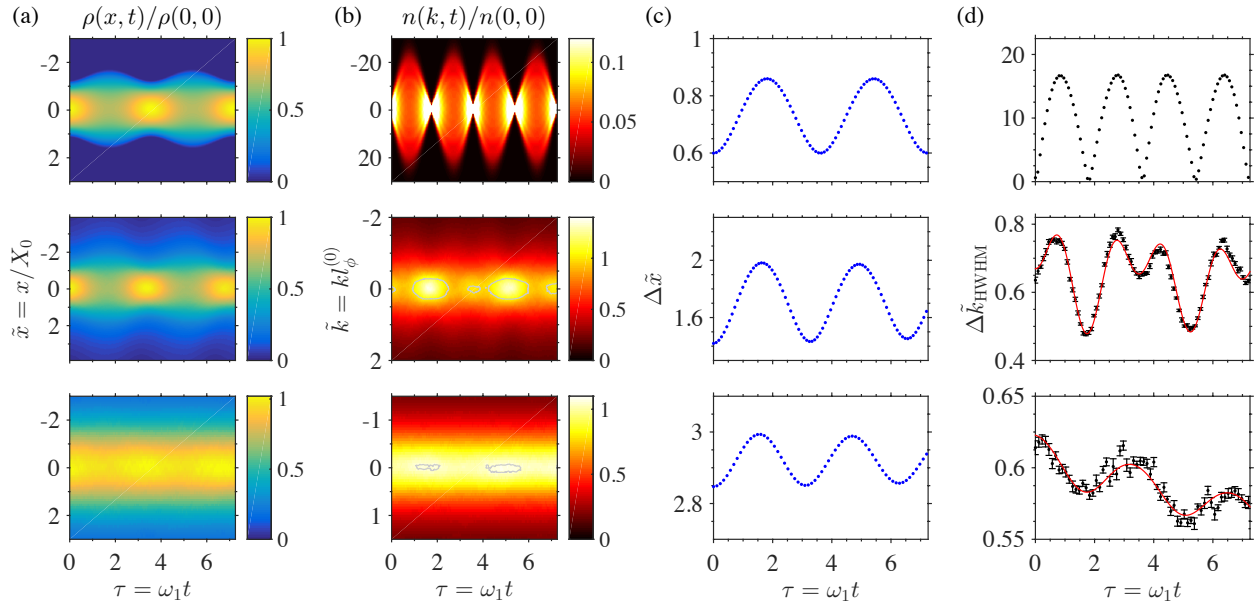


FIG. 1. (Color online). Results of PGPE simulations illustrating the breathing mode oscillations of a harmonically trapped, weakly-interacting 1D Bose gas after a confinement quench. (a) Density; (b) momentum distribution; (c) rms width $\Delta\tilde{x}$ of the density; and (d) half-width-at-half-maximum $\Delta\tilde{k}_{\text{HWHM}}$ of the momentum distribution; all as a function of the dimensionless time $\tau = \omega_1 t$. The three examples correspond, respectively, to: $\epsilon = 0.563$, $A = 104$, $t_0 = 10^6$ and $\hbar\omega_0/[g\rho_0(0)] = 3.0 \times 10^{-3}$ – top row; $\epsilon = 0.778$, $A \approx A_{\text{fd}} = 2.3$, $t_0 = 10^3$, and $\hbar\omega_0/[g\rho_0(0)] = 0.07$ – middle row; and $\epsilon = 0.1$, $A = 1.15$, $t_0 = 10^6$, and $\hbar\omega_0/[g\rho_0(0)] = 0.1$ – bottom row. In (d) the black points are *c*-field data, with the error bars indicating 95% confidence intervals, whilst the solid red curves are fits of the form $B_1 \exp(-b_1 t)[\sqrt{K} \cos(\nu t) - \sqrt{1 - K} \cos(2\nu t)] + B_2 \exp(-b_2 t)$.

The equilibrium momentum distributions generated by SPGPE differ slightly to those generated from Eq. (10) of the main text. This is not unexpected; various assumptions that go into Eq. (10) (such as a Thomas-Fermi density profile and the LDA) are relaxed in SPGPE. A fairer comparison to our finite-temperature hydrodynamic theory is therefore obtained

by fitting the equilibrium momentum distribution predicted by Eq. (10) of the main text to the *c*-field equilibrium momentum distribution (with A and $\hbar\omega_0/[g\rho_0(0)]$ as free parameters). This shifts the dataset $(A, K) \rightarrow (A', K)$; the *c*-field values of A_{fd} reported in Fig. 1 of the main text are computed with respect to this latter dataset.

[1] Explicitly, the dimensionless function \mathcal{N} for a 1D Bose or Fermi gas is given by $\mathcal{N}((\hbar^2 k^2/2m - \mu)/k_B T) = \frac{1}{2\pi} [e^{(\hbar^2 k^2/2m - \mu)/k_B T} \mp 1]^{-1}$, i.e., it is proportional to the Bose-Einstein (–) or Fermi-Dirac (+) distribution function, respectively.

[2] P. B. Blakie, A. S. Bradley, M. J. Davis, R. J. Ballagh, and C. W. Gardiner, *Advances in Physics* **57**, 363 (2008).

[3] C. W. Gardiner, J. R. Anglin, and T. I. A. Fudge, *Journal of Physics B: Atomic, Molecular and Optical Physics* **35**, 1555 (2002).

[4] C. W. Gardiner and M. J. Davis, *Journal of Physics B: Atomic, Molecular and Optical Physics* **36**, 4731 (2003).

[5] M. J. Davis, R. J. Ballagh, and K. Burnett, *Journal of Physics B: Atomic, Molecular and Optical Physics* **34**, 4487 (2001).

[6] M. J. Davis, S. A. Morgan, and K. Burnett, *Phys. Rev. Lett.* **87**, 160402 (2001).

[7] A. Sinatra, C. Lobo, and Y. Castin, *Journal of Physics B: Atomic, Molecular and Optical Physics* **35**, 3599 (2002).

[8] T. P. Simula, M. J. Davis, and P. B. Blakie, *Phys. Rev. A* **77**, 023618 (2008).

[9] A. Bezett and P. B. Blakie, *Phys. Rev. A* **79**, 023602 (2009).

[10] A. S. Bradley, P. B. Blakie, and C. W. Gardiner, *Journal of Physics B: Atomic, Molecular and Optical Physics* **38**, 4259 (2005).

[11] P. B. Blakie and M. J. Davis, *Phys. Rev. A* **72**, 063608 (2005).

[12] S. J. Rooney, P. B. Blakie, and A. S. Bradley, *Phys. Rev. E* **89**, 013302 (2014).

[13] Y. Castin, R. Dum, E. Mandonnet, A. Minguzzi, and I. Carusotto, *Journal of Modern Optics* **47**, 2671 (2000).

[14] I. Bouchoule, M. Arzamasovs, K. V. Kheruntsyan, and D. M. Gangardt, *Phys. Rev. A* **86**, 033626 (2012).